JOURNAL OF MATERIALS SCIENCE 35 (2000) 2529–2538

Aging impact on mechanical properties and microstructure of Al-6063

A. MUNITZ, C. COTLER
Nuclear Research Center-Negev, P.O. Box 9001, Israel
E-mail: moniz@mail.mofet.macam98.ac.il

M. TALIANKER
Department of Material Sciences, Ben Gurion University, Beer-Sheva, Israel

The impact of aging on the mechanical properties and microstructure of Al-6063 alloys were studied, using scanning and transmission electron microscopy, as well as tensile measurements. It was found that the 0.5% yield stress and the ultimate tensile strength increase at the beginning of the aging process, reach a maximum, and than decrease with increasing the aging duration. On the other hand, the uniform elongation, the total elongation, and the strain hardening factor decrease with increasing aging duration well after the material reaches the maximum strength (T6 conditions), reaches a minimum and than increase again. The final fracture area reduction also decreases to a minimum, which occurs simultaneously with the maximum of the ultimate tensile strength; then it increases with aging time. The final fracture area reduction is accompanied with morphology transition from transgranular shear rupture to a combination of transgranular shear rupture and intergranular dimpled structure. The intergranular rupture area increases with aging up to the minimum in the total elongation, and then decreases with aging duration. Aging is accompanied with the appearance of needle-like Mg_2Si precipitates except in Precipitation Free Zones (PFZ) that are adjacent to the grain boundaries. The PFZ size depends on the annealing temperature, while the morphology and density of the precipitates depend on the annealing duration. A correlation has been established between the PFZ and the measured mechanical properties and fracture morphology. The impact of the Mg/Si ratio on the mechanical properties is discussed.

1. Introduction

Aluminum alloys are extensively used as structural materials in the nuclear industry such as in fuel cladding and reactor cores because of their good corrosion resistance and very low capture cross-section for fast and thermal neutrons. In the past, the choice of a particular alloy for use as a structural material was based on the measured properties of the unirradiated material [1]. Naturally, structural materials in a reactor core are exposed to large fluxes of fast and thermal neutrons, and are exposed to temperature fields of approximately 50°C for very long duration. This should result in changes in the microstructural and mechanical properties. Numerous studies have been performed concerning irradiation impacts on the properties of aluminum alloys [1–8]. However very meager information exists on the impact of prolong exposure to temperature fields (50°C). It was found that irradiation of cold-worked Al-A5 causes its annealing, and as a result the ultimate tensile strength and elongation increase with the neutron fluence [9]. Some studies indicate that annealing of cold worked Al-1100 [10] and Al-6061 [1] may also occur during irradiation.

In a previous work it was found that prolonged annealing of cold worked Al-6063 at 50°C revealed similar results to those of irradiation under specific conditions (thermal and fast neutron fluxes of the order of 10^{13} $ncm^{-2}s^{-1}$) [11]. Therefore, knowledge of the impact of aging on the mechanical properties and microstructure will be of great help in analyzing the irradiation effects on Al-6063. The present work is aimed at investigating the aging characteristics of Al-6063 and the impact of aging on the mechanical properties as well as on the internal microstructure.

2. Experimental

Al-6063 tubes 1 mm in thickness were hot extruded from 480°C followed by water quenching. Two different Al-6063 compositions were examined containing different Mg levels yet identical Si ones, as listed in Table I.

Tensile specimens: 50 mm long and 6 mm wide gauge sections, were punched out from the as extruded tubes. The tensile specimens as well as transmission electron microscopy-TEM specimens were inserted into a

TABLE I Composition of two Al-6063 batches used in the present investigation

Element	Batch I [wt.%]	Batch II [wt.%]
Fe	0.42	0.50
Si	0.18	0.18
Mg	0.51	0.64
Mn	0.03	0.04
Cu	0.01	0.01
Zn	0.01	0.01

furnace for aging at different temperatures and durations. Then, the tensile specimens were tensioned till fracture in an Instron tensiometer at a strain rate of 2×10^{-2} mm/s. At least three specimens were tensioned at each point. Fractured surfaces were examined with a scanning electron microscope. TEM specimens were thinned for transmission electron microscopy. First, thinning to about 150 μm was performed chemically with a 1 M aqueous solution of NaOH. Then discs of 3 mm diameter were punched out of the specimen, and further thinned by electropolishing using an electrolyte comprising of 20% perchloric acid in methanol at $-20\,^{\circ}$C, at a voltage of 20–30 V.

3. Results

3.1. Mechanical properties

A summary of the mechanical properties of Al-6063 of batch I aged from the as-extruded state at 175°C for different durations, or aged for 5.5 hrs at different temperatures are given in Tables II and III, respectively. A series of graphs illustrating the 0.5% yield stress, σ_Y, the ultimate tensile stress, σ_{UTS}, the uniform elongation, the total elongation, and the strain hardening factor for specimens aged from the as-extruded state at 175°C for different durations, or aged for 5.5 hrs at different temperatures, are presented in Figs 1 and 2, respectively. As can be seen from Figs 1 and 2 and Tables II and III, the 0.5% yield stress and the ultimate tensile strength

TABLE II Mechanical properties of Al-6063 from Batch I aged at 175°C for different durations

Aging duration [hrs]	Stress		Elongation		Strain hardening factor [n]
	σ_Y [MPa]	σ_{UTS} [MPa]	Uniform [%]	Total [%]	
0	90	171	17.4	20.6	0.211
1	109	184	15.9	18.8	0.169
2	128	196	13.81	17	0.132
3	149	208	12.46	16.21	0.111
4	174	217	10.9	14.82	0.096
5	188	228	10.19	13.68	0.087
6	200	235	9.3	12.85	0.084
8	208	239	8.97	11.6	0.079
16	212	241	7.6	9.1	0.069
20	214	242	7.3	8.5	0.067
24	216	243	7	8	0.066
40	207	230	6.3	7.14	0.068
48	203	225	6	6.8	0.071
64	199	220	5.9	6.4	0.079
72	197	218	5.7	6.3	0.084

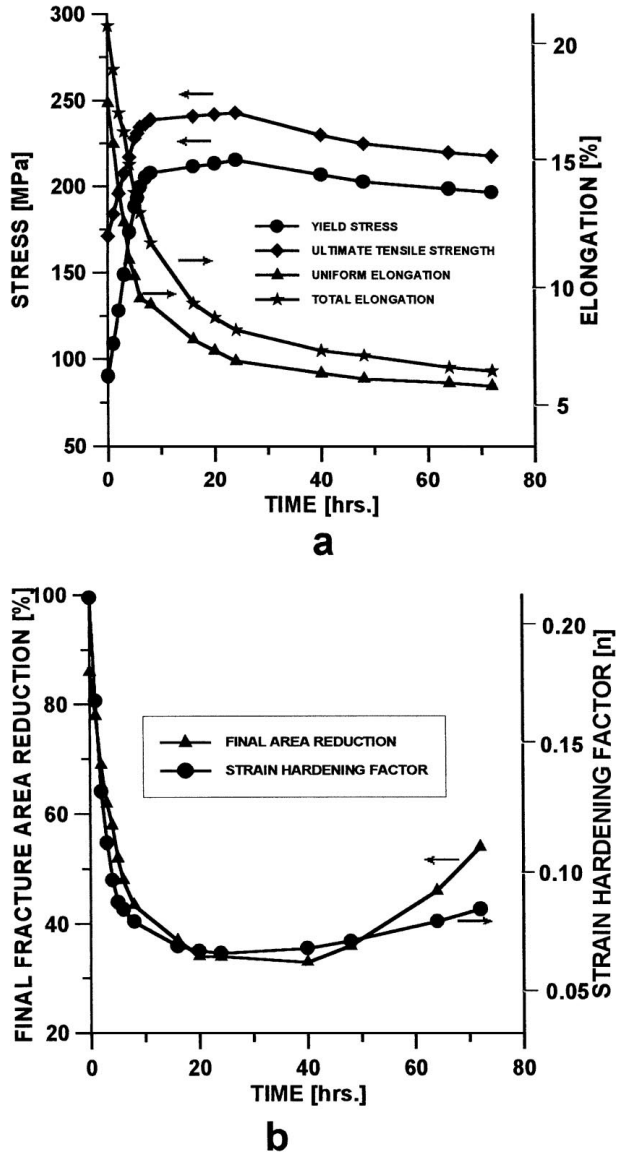

Figure 1 Mechanical properties of Al-6063 aged at 175°C for different temperatures. a) 0.5% yield stress, ultimate tensile stress, uniform elongation, total elongation. b) strain hardening factor, final area reduction.

increase at the beginning of the aging process, reach a maximum by the T6 conditions, and than decreases with increasing aging time or with the aging temperature. On the other hand, the uniform elongation, the total elongation, the final area reduction at fracture, and the strain hardening factor, decrease with increase of the age process well after the material reaches the maximum strength (T6 conditions), they reach a minimum, and than increase again. The final area reduction has a maximum simultaneously with the maximum of the ultimate tensile strength.

In general, the mechanical properties behavior for aging at a certain temperature for different durations are similar to the behavior under heating for a constant time, yet at different temperatures. Therefore, one can speak of an aging state, which can be achieved in different ways while obtaining similar mechanical results.

The impact of the Mg/Si ratio on the mechanical properties is seen in Fig. 3. Changing the Mg/Si ratio from 2.78 to 3.56 did not change the general behavior of the mechanical properties. However, there are

TABLE III A summary of the mechanical properties of Al-6063 from Batch I aged for 5.5 hrs at different temperatures

Temperature [°C]	Stress		Elongation		PFZ	Strain hardening factor [*n*]	Final area reduction
	Yield [MPa]	UTS [MPa]	Uniform [%]	Total [%]			
150	162	230	15.6	20.2	140	0.174	
160	185	239	13.5	17.2	190	0.152	85
175	215	251	10.1	12.9	210	0.089	55
185	221	250	8.3	10.7	290	0.072	40
190	222	244	7.4	9.6	330	0.064	45
200	200	224	5.8	7.1	340	0.062	57
210	173	205	6.1	7.6	360	0.084	
220	150	184	6.4	9.2	450	0.103	
230	133	170	6.8	10.7		0.118	85
240	120	162	7.4	12.6	310	0.134	

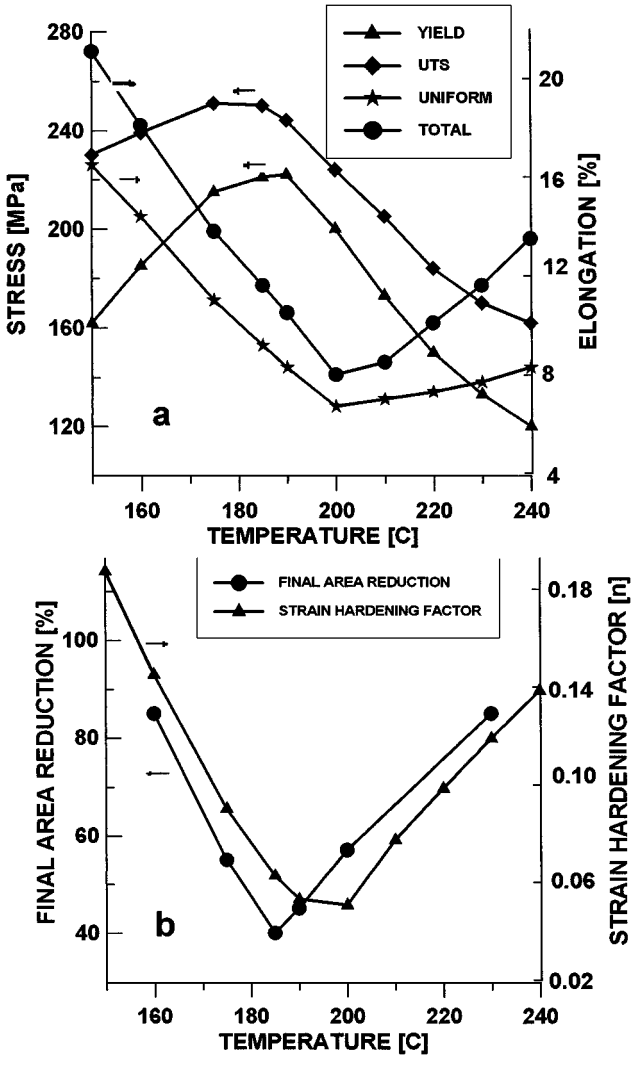

Figure 2 Mechanical properties of Al-6063 aged at different temperatures for 5.5 hrs. a) 0.5% yield stress, ultimate tensile stress, uniform elongation, total elongation. b) strain hardening factor, final area reduction.

differences in the absolute values. For example, the yield stress and the ultimate tensile strength of the Al-6063 with Mg/Si ratio of 3.56 is higher than these for the Mg to Si ration of 2.78. Only at very long aging duration the difference disappears. In contrast, the elongation (uniform and total) of Al-6063 with the lower Mg/Si ratio is larger than those for Al-6063 with lager

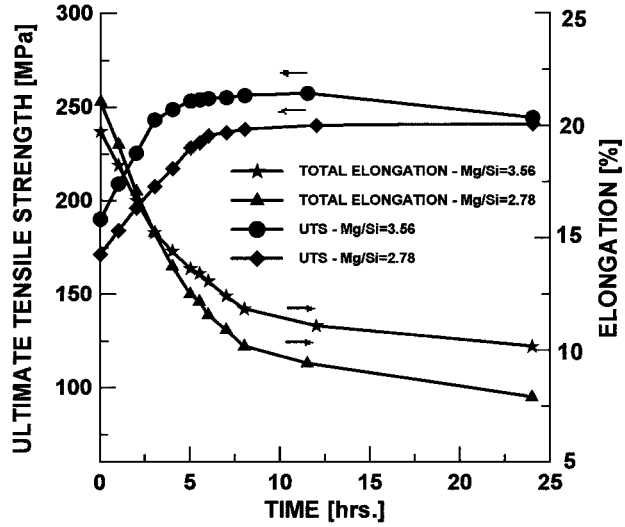

Figure 3 Impact of the Mg to Si ration on the ultimate tensile strength and total elongation for Mg/Si = 3.56 (batch II) and for Mg/Si = 2.78.

Mg/Si ratio at the early aging stages. This behavior is reversed for aging times longer than 5 hrs.

3.2. Fracture morphology

Fracture morphologies for Al-6063 aged at 175°C for different aging duration and for Al-6063 aged 5.5 hrs at different temperatures are illustrated in Figs 4 and 5, respectively. The fracture of the as-extruded samples exhibits a transgranular dimpled shear rupture microstructure (Fig. 4a and 4b). This morphology is characteristic of ductile fracture. The local area reduction is defined as the final rupture area divided by the undeformed cross-sectional area. Since the observation indicates that the deformation occurred mainly through decreasing in thickness while the specimen width remain almost unchanged, one can use the ratio between the final rupture thickness (marked on the figure) to the original thickness as an approximation for the area reduction. As seen in Fig. 4, the final area reduction first decreases with aging (increase in the final rupture thickness), reaching a minimum and than increases again. The change in the final rupture area is accompanied with change in the fracture morphology. Due to aging, the fracture morphology changes to a mixture of transgranular dimpled shear rupture and dimpled

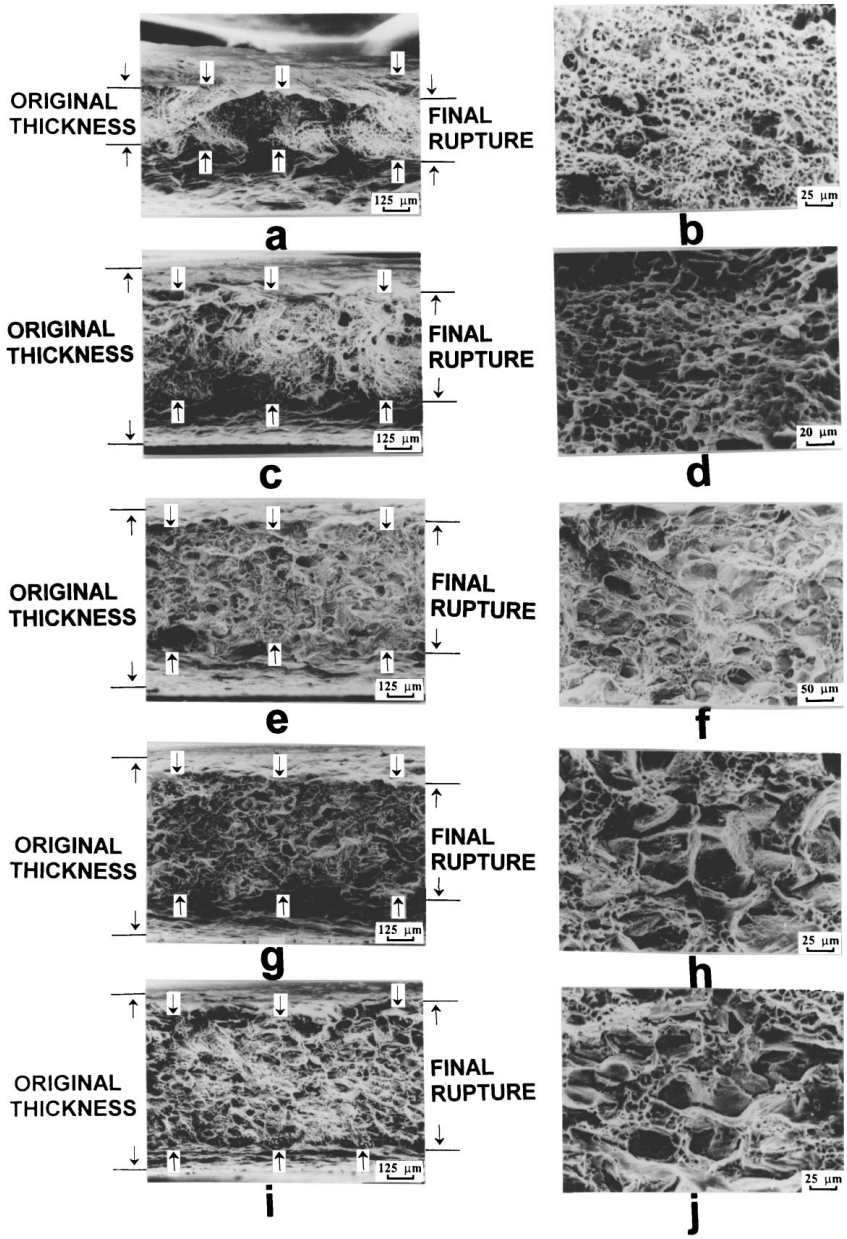

Figure 4 Secondary electron images illustrating the microstructure of Al-6063 aged for 175°C for different times. a, b) 1 hrs. c, d) 4 hrs. e, f) 8 hrs. g, h) 64 hrs. i, j) 72 hrs.

intergranular rapture which appears as large facets in Fig. 4h. The proportion of the dimpled intergranular rupture areas increases with aging time up to 64 hrs of aging. Further aging causes an increase in the local area reduction. This is accompanied with a decrease in the intergranular facets (compare Fig. 4h with 4j). The same phenomenon was observed for aging by 5.5 hrs for different temperature as illustrated in Fig. 5. The local area reduction as a function of temperature is plotted in Fig. 1d. One may correlate the fracture morphology with the strain-hardening factor as illustrated in Fig. 6. The amount of the intergranular fracture increases with decrease of the strain intensity factor.

In Fig. 7 we present secondary electron images illustrating the facet morphology at two magnifications. At a lower magnification the fracture looks brittle. However, at a larger magnification, the facets reveal a dimpled structure (Fig. 7b). The size of the dimples on the facets are by an order of magnitude smaller than the dimples revealed in the shear transgranular rupture zones.

3.3. Internal microstructure

Aging of Al-6063 caused internal microstructure changes. Usually, after a certain aging state one could observe needle like precipitates inside the entire grains, except for the area adjacent to the grain boundary where a precipitation free zone (PFZ) could be observed. The nature of precipitation and the PFZ in Al-6063 is presented in Figs 8 through 11. Bright-field transmission electron images illustrating the internal microstructure of Al-6063 aged for 5.5 hrs at different temperatures are presented in Fig. 8. After aging of 150 hrs at 150°C, precipitates are barely seen Fig. 8a. The bright and dark line contrast is probably the stress field due to dislocation loops. The surface modulation of tiny black-and-white contrast is probably caused by precipitation. Aging for 5.5 hrs at 190°C caused the appearance of massive

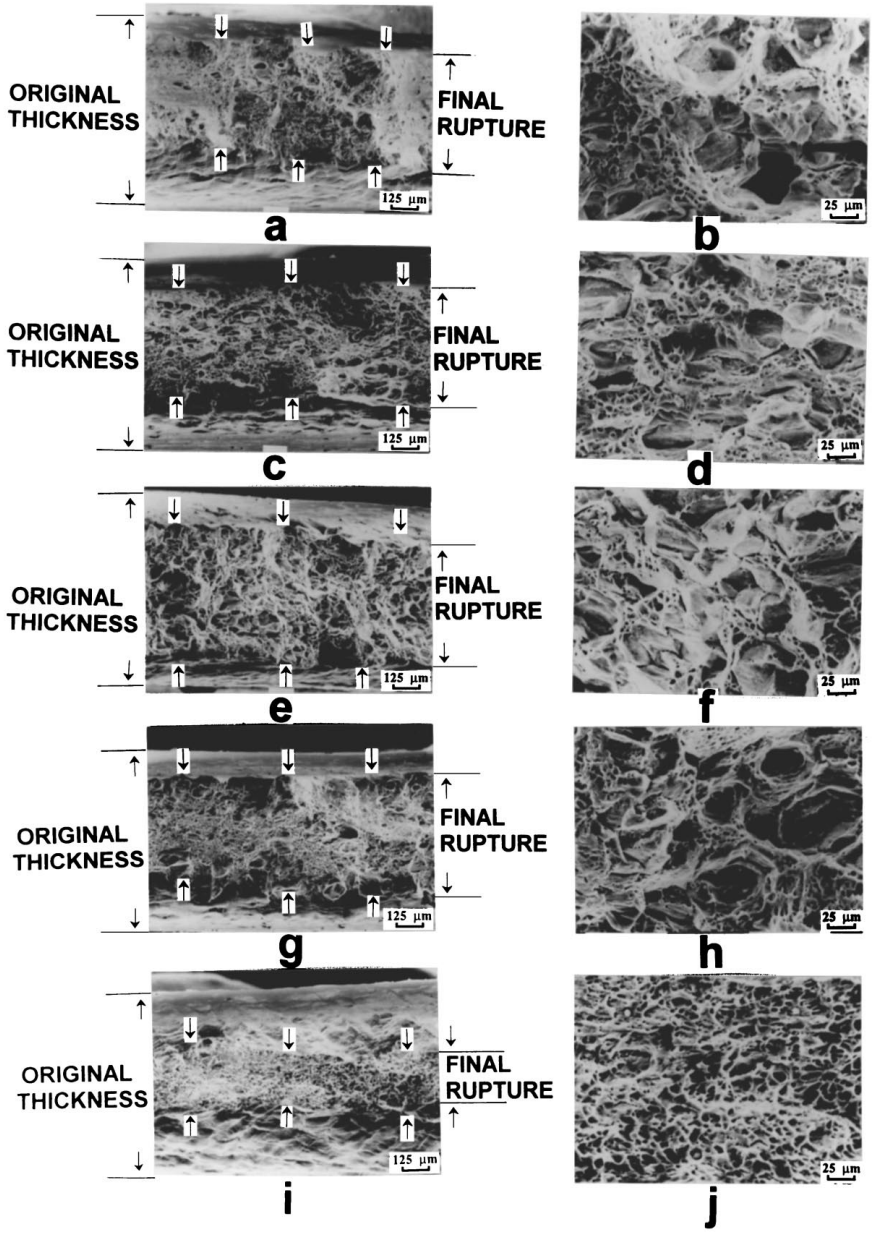

Figure 5 Secondary electron images demonstrating the microstructure of Al-6063 aged for 5.75 hrs at different temperatures. a, b) 165°C, c, d) 170°C, e, f) 182°C. g, h) 185°C. i, j) 220°C. °Cc.

needle precipitation in two perpendicular directions. These precipitations were identified, according to their morphology, as Mg_2Si [12]. On the other hand, aging at 240°C for 5.5 hrs caused the appearance of a lower density of massive Mg_2Si precipitates, as compared to those which appeared after aging at 190°C for 5.5 hrs. A similar sequence was observed when aged at 175°C for different durations, as illustrated in the bright-field transmission electron images in Fig. 9. After aging at 175°C for 2 hrs one can observe the early stages of precipitation—the dark points in the lower right of Fig. 9a. A grain boundary could be observed in the center of Fig. 9a, while on the right side one observes the begging of the PFZ creation. After aging for 5.5 hrs the dimension of the needle shaped precipitation is observed, and a well developed PFZ may as well be seen on both sides of the grain boundary (Fig. 9b). After aging for 64 hrs, coarser Mg_2Si precipitates of a lower density appear, which is characteristic to overaging conditions as will be discussed later. It was found that for the same aging temperature one obtains the same PFZ size regardless of the aging duration, as demonstrated for aging at 175°C in Fig. 9. In contrast, aging at different temperature has an impact on the PFZ size. Decreasing the aging temperature decrease the PFZ as can be seen in Fig. 10. The measured PFZ for the different aging temperatures is summarized in Table IV. The maximum strength is obtained after reaching the T6 condition, which depends on the aging temperature and is indicated in parentheses adjacent to the aging time. However, increasing the temperature above 210°C caused penetration of the precipitates into the PFZ. It is therefore difficult to obtain a PFZ near a grain boundary as illustrated in Fig. 11.

Transmission electron images illustrating the microstructure of the PFZ and its vicinity after tension was applied are presented in Fig. 12. As seen, larger dislocation density appears inside the PFZ.

TABLE IV A summary of the mechanical properties of Al-6063 from Batch I aged for 5.5 hrs at different temperatures including the precipitation free zone (PFZ)

Temperature [°C]	Stress		Elongation		PFZ [nm]	Strain hardening factor [*n*]
	Yield [MPa]	UTS [MPa]	Uniform [%]	Total [%]		
150 (150)	239	275	9.8	12.2	140	0.082
160 (48)	238	263	8.1	12.2	190	0.064
175 (12)	228	254	7.1	10	210	0.069
185 (5)	228	258	7.9	11	310	0.072

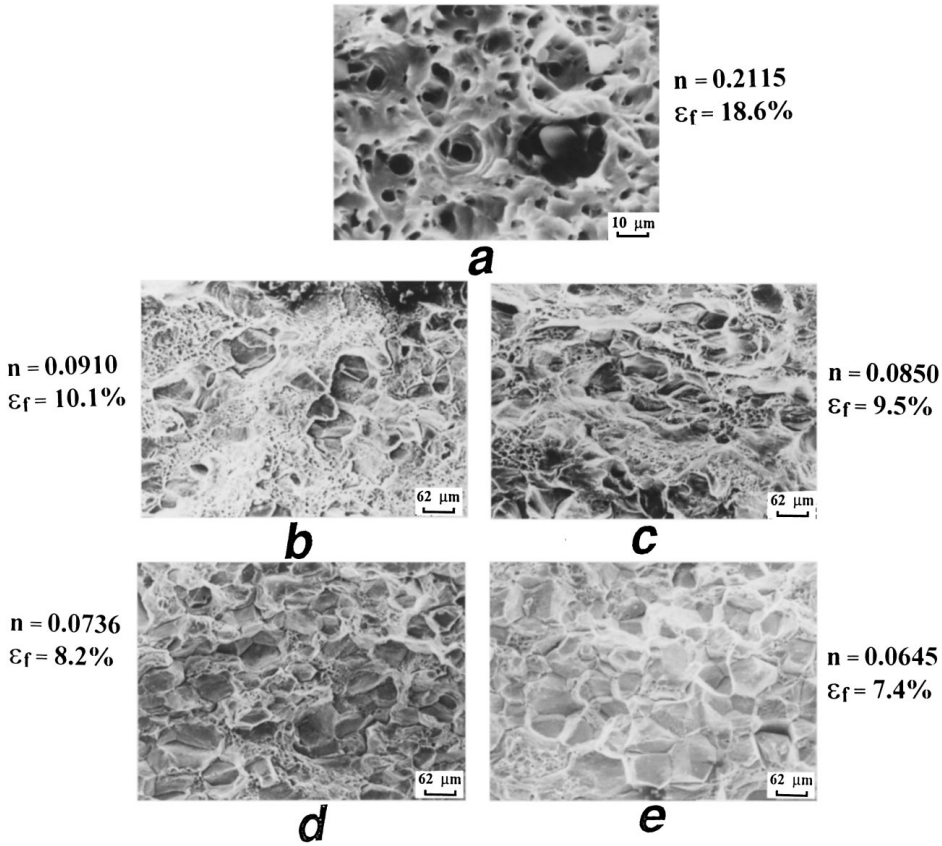

Figure 6 Secondary electron images demonstrating a correlation between the fracture morphology with the strain-hardening factor.

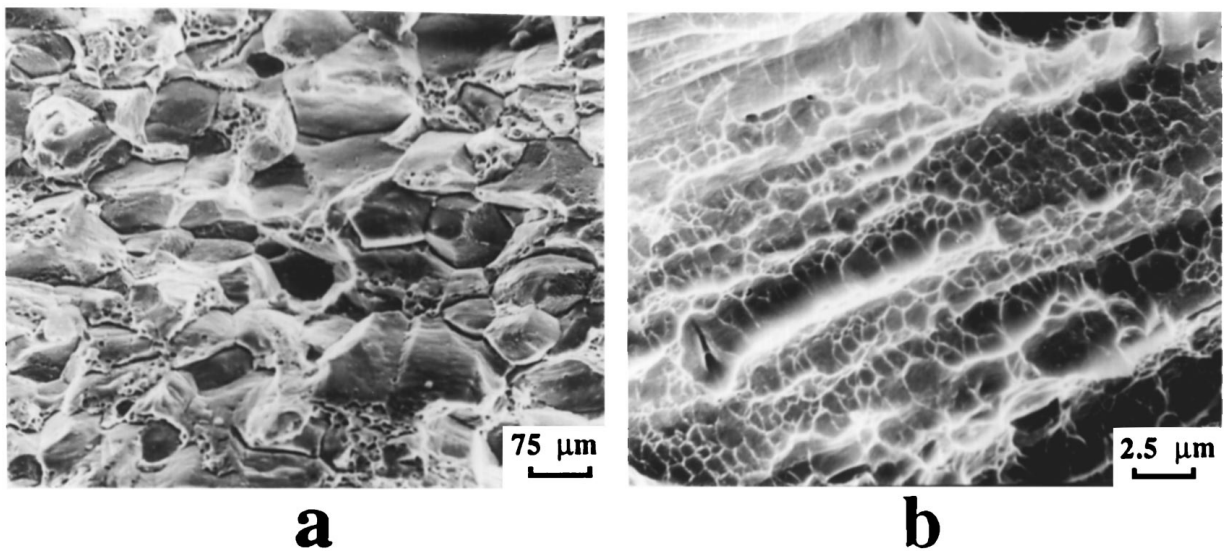

Figure 7 Secondary electron images demonstrating the nature of the intergranular facets at two magnification.

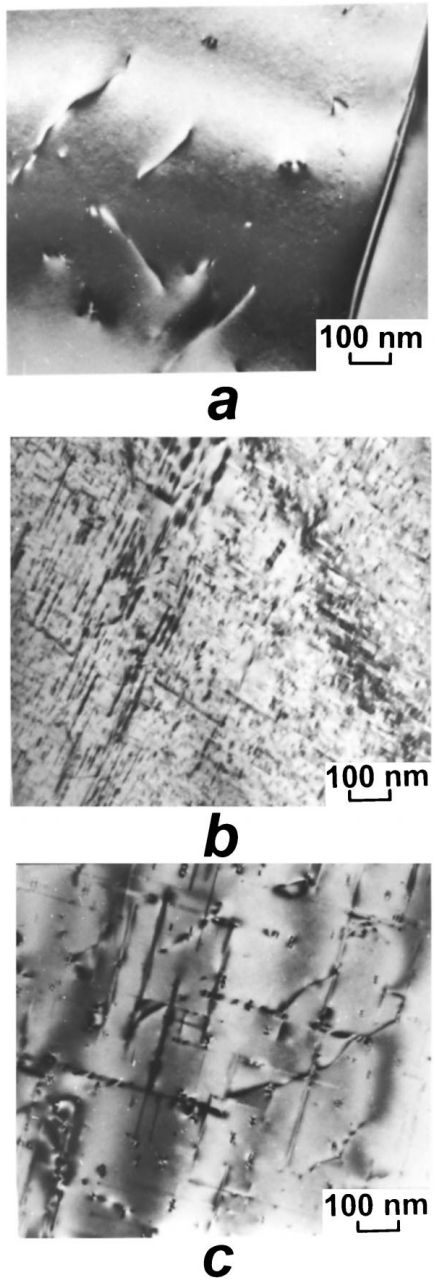

Figure 8 Bright-field transmission electron images illustrating the internal microstructure of Al-6063 aged for 5.5 hrs at different temperatures. a) 150°C, b) 190°C, and c) 240°C.

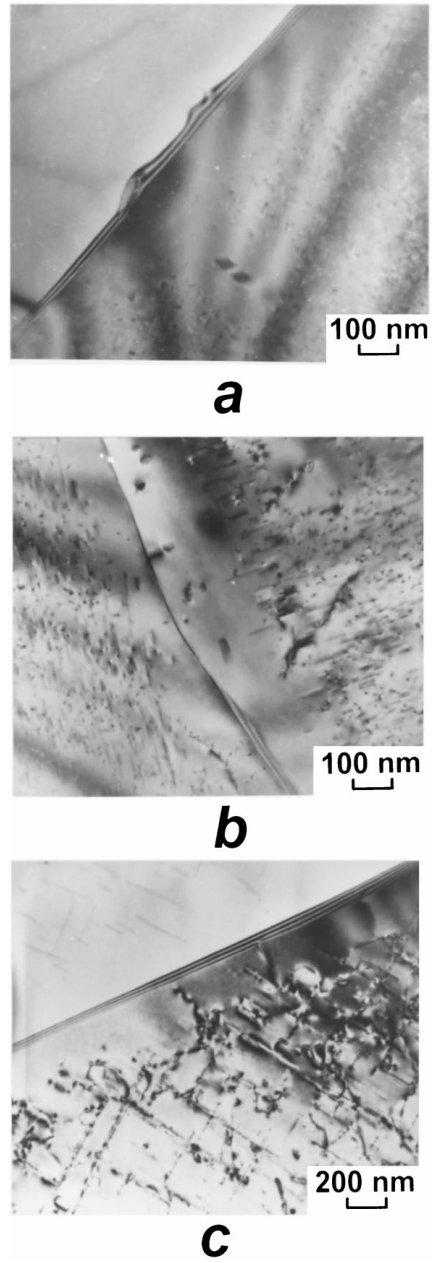

Figure 9 Bright-field transmission electron images illustrating the internal microstructure of Al-6063 aged at 175°C for different duration. a) 2 hrs. b) 5 hrs. c) 64 hrs.

4. Discussion

Extrusion of Al parts at 480°C causes the formation of a solid solution of Mg and Si in the Al lattice. Aging of the supersaturated Al solid solution at elevated temperatures induces solid state precipitation according to the following sequence [12]:

$$\text{solid solution} \longrightarrow \text{GP zones} \longrightarrow \text{Mg}_2\text{Si}'' \longrightarrow \text{Mg}_2\text{Si}' \longrightarrow \text{Mg}_2\text{Si} \qquad (1)$$

The precipitation starts with the formation of spherical GP zones, which essentially are enriched Mg and Si zones. The formation of GP zones is usually followed by the precipitation of so-called transition phases. As aging continues the GP zones elongate in the [100] matrix direction, and assume a needle-like shape, 16 to 200 nm long, with a monoclinic structure (β'' structure). The needles grow to become rods (β' structure, of a cubic lattice) and eventually transform to Mg_2Si platelets. These microstructural changes taking place during aging also induce mechanical properties changes. In general, the precipitation causes strengthening. Immediately after extrusion, the main resistance to dislocation movement is solid solution hardening. The specimen is relatively easily deformed at this stage, and the hardness is low. At this stage, a fully transgranular dimpled structure is obtained, with a maximum in elongation and a low tensile strength. As GP zones form, the hardness increases due to the extra stress required forcing dislocations through the coherent zones. The tensile strength continues to increase with the formation of coherent β'' precipitates, because now the dislocation must be forced through the highly strained matrix

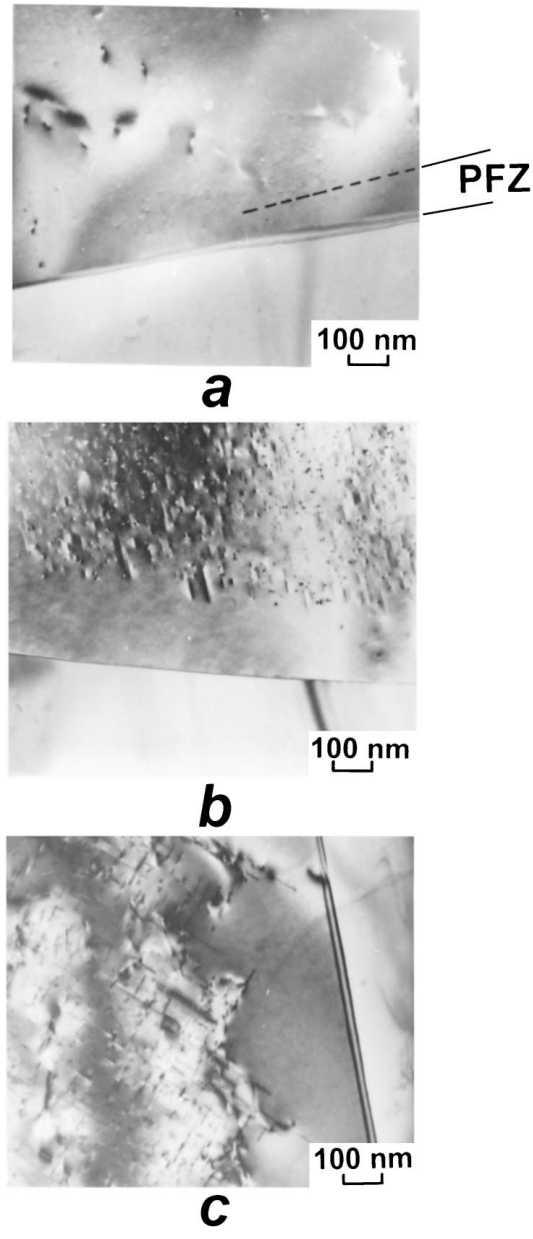

Figure 10 Bright-field transmission electron images illustrating the precipitation free zone-PFZ of Al-6063 aged at different temperatures. a) 150°C, b) 175°C, and c) 190°C.

that results from the misfit perpendicular to the β'' precipitates. However, at the beginning of the aging process, the thickness of the β'' precipitates is small and the dislocation can shear them very easily. As aging continues the needle-like β'' (Mg_2Si'') become thicker and transform to β' (Mg_2Si') rods. Therefore, the force needed for precipitate shearing becomes larger, hence an increase in strength and a lower elongation. As aging continues, the β' (Mg_2Si') become coarser and eventually transform to β (Mg_2Si) platelets. As the β' (Mg_2Si') thicken the precipitate density decreases, hence the inter-particle distance increases. Nevertheless, the distance is still sufficiently small to cause an increase in ultimate tensile strength. The maximum strength is gained just before the rods transform in to platelets (T6 conditions). At this stage, the precipitates coarsen, which results in a lower particle density, hence a larger distance between particles. The dislocations then can squeeze themselves between the precipitates. Such a process requires less force for dislocation movement, hence a lower strength and increase in elongation.

Usually, during aging Mg_2Si precipitates throughout the entire grain, while at the grain boundary a precipitation-free zone (PFZ) is formed. There are two main reasons for the PFZ formation:

(i) Mg diffusion into the grain boundary causing the formation of big Mg_2Si precipitates at the grain boundary. The latter mechanism has not been observed in our case.

(ii) Vacancy diffusion into the grain boundary and a formation of vacancy depleted zone near a grain boundary. An excess of vacancies in the Al lattice is essential for starting off the precipitation process. For example, GP zones in Al-Cu can be formed by aging at room temperature, which would not be feasible without the assistance by an excess of vacancies [13]. The vacancy excess, in our case, is achieved by quenching from the extrusion temperature to room temperature. Since vacancies have a high diffusivity, it is difficult to avoid losing vacancies in the vicinity of grain boundaries.

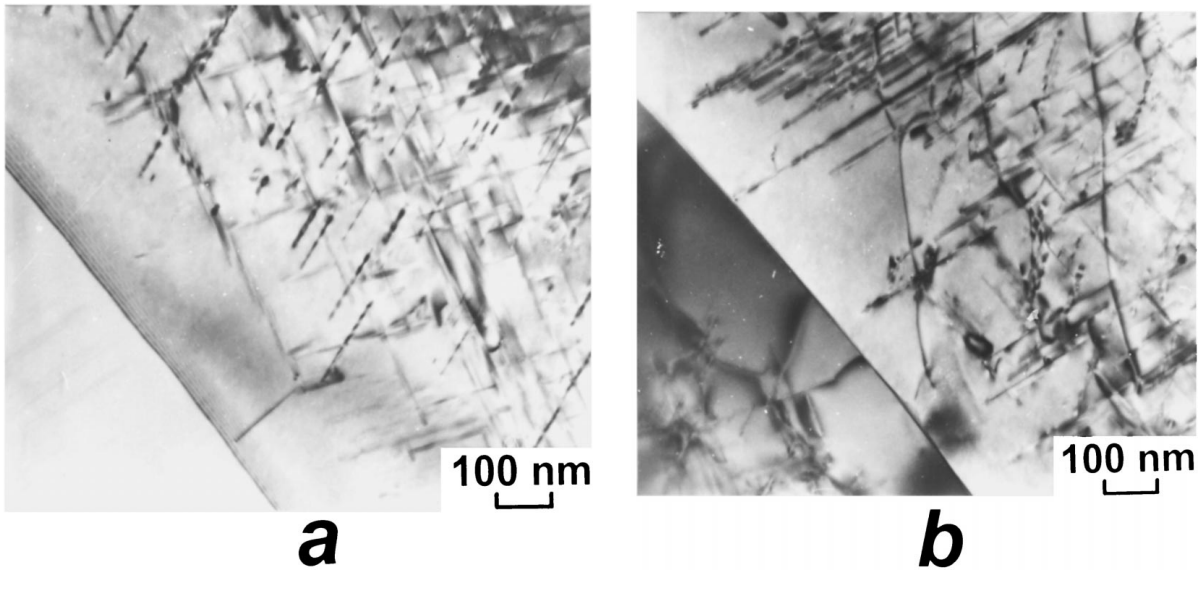

Figure 11 Bright-field transmission electron images illustrating the precipitation free zone-PFZ of Al-6063 aged at 210°C for 5.5 hrs. at two locations.

Therefore, close to the grain boundary the vacancy concentration will correspond to thermal equilibrium at the aging temperature. Away from the boundary, it will correspond to the solution treatment. As a result, Mg_2Si precipitates could be formed in the grains and not in grain boundaries, hence the precipitation-free zone-PFZ. Theoretically [13], at low aging temperatures, where the driving force for precipitation is high, the critical supersaturation needed for precipitation is lower and narrower PFZs are formed. This was confirmed in our investigation as can be seen in Table IV. Aging at 150°C and 185°C creates a PFZ with a width of 140 and 310 nm, respectively. As will be discussed in the next paragraph, the size of the PFZ has a great impact on the mechanical properties.

The formation of the PFZ near the grain boundary might explain the formation of transgranular dimpled structure after aging. Since the PFZ is weaker than the grain it reasonable to assume that the fracture will take place inside the PFZ. As a results of the crack propagation inside the PFZ one obtained the faceted phase. However, it was found that the Mg_2Al precipitates protrude into the PFZ (Fig. 9). These protruding precipitates serve as the nucleation sites for the formation of dimples. Therefore, a transgranular-dimpled structure is obtained.

As can be seen in Fig. 12 the PFZs are playing a great deal during tension. The dislocation density after tension in the PFZ is much higher than the density in the grains. Therefore we believe that strain hardening is taking place during tension in the PFZ. On the other hand, due to aging precipitates are formed in the grains, which increase the grain strength. Increasing the PFZ and grain strength will cause an increase in the ultimate tensile strength as well as in the uniform elongation. It is intuitively understood that the dislocation density in a narrow PFZ will be higher than that for a broader PFZ. Therefore, larger strain hardening is expected (i.e.) in a narrower PFZ, hence larger ultimate tensile strength before necking. Therefore, it is expected that both the ultimate tensile strength and the uniform elongation will be lager for smaller PFZ than these for larger PFZ, as actually was observed as demonstrated in Table IV. For example, aging at 150 and 185°C until the maximum strength is obtained (different aging duration for each temperature) will result in a PFZ of 140 and 210 nm, an ultimate tensile strength of 275 and 254 MPa, and an uniform elongation of 9.8 and 8.1%, respectively. On the other hand, the total elongation is comprised of two contributions: the uniform elongation and the elongation due to necking. Since at T6 conditions there is a minimum in final area reduction of the fracture there will be a minimum of the contribution to the total elongation. Therefore it is not surprising that even though the uniform elongation increases there is a decrease in the total elongation.

The creation of PFZ zones might be the reason why Alexander [14] found large crack propagation in spite of only minor changes in the fracture toughness. A similar explanation of the fracture morphology was given by Sturcken [15].

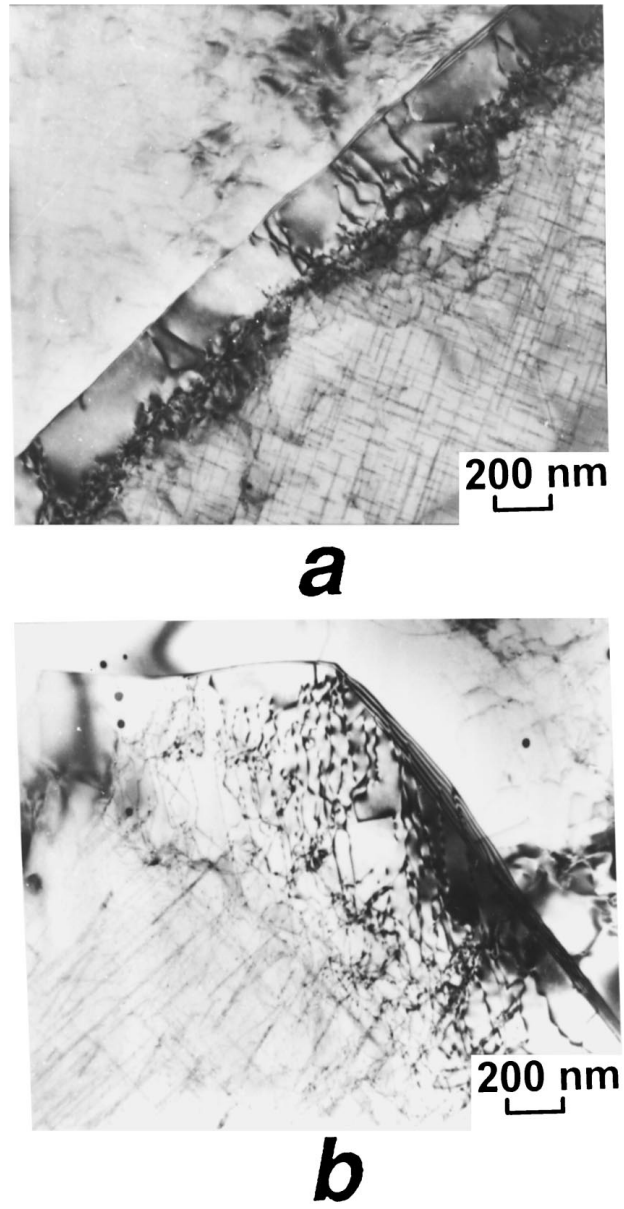

Figure 12 Bright-field transmission electron images illustrating the precipitation free zone-PFZ of Al-6063 aged at 185°C for 5.5 hrs after applying tension at two locations.

One has to look at the aging condition as physical state. For each state exists a group of mechanical properties, such as yield strength, ultimate tensile strength, uniform and total elongation, strain hardening factor, and final fracture reduction. One can choose the aging temperature and duration in order to get a certain group of mechanical properties. As can be seen in Figs 1 and 2, for a certain yield stress or ultimate tensile strength one can have two values of elongation. If the strength is the important property than one would choose the T6 condition while if elongation is more important one need to choose under aging condition where one would get a little lower strength with much more elongation.

5. Summary and conclusions

The present work yields the following findings:

Annealing of Al-6063 induces the 0.5% yield stress and the ultimate tensile strength increases at the

beginning of the aging process, reaches a maximum, and than decreases with increasing the aging time. On the other hand the uniform elongation, the total elongation, and the stress intensity factor are decreasing with increasing the age process well after material reaches the maximum strength (T6 conditions), reaches a minimum and than increases again. The fracture of the fully annealed condition is fully transgranular shear dimpled structure. As the aging process continues, there is a decrease in the local area reduction of the final fracture, up to a minimum. At this point the local area reduction begins to increases. The area reduction is accompanied with morphology transition from transgranular shear rupture to a combination of transgranular shear rupture with intergranular dimpled structure. The intergranular rupture area increases with aging process up to the maximum aged condition (T6) and than decreasing with overaging conditions. The internal microstructural changes occurred during the aging process were correlated with the measured mechanical properties and the fracture morphology.

Acknowledgements

The authors wish to thank to Dr. Z. Burshtein for his critical reading of the manuscript.

References

1. R. T. KING and A. JOSTSONS, *Met. Trans. A* **6a** (1975) 863.
2. H. E. MCCOY, JR and J. R. WEIR, JR, *Nucl. Sci. and Eng.* **25** (1966) 319.
3. N. H. PACKAN, *J. Nucl. Mater.* **40** (1971) 1.
4. A. JOSTSONS and E.L. LONG, JR., *Radiation Effects* **16** (1972) 83.
5. R. T. KING, A. JOSTSONS and K. FARRELL, in Proc. Effects of Radiation on Structure and Mechanical Properties of Metals and Alloys, ASTM STP 529 (American Society for Testing and Materials, 1973) p. 165.
6. K. FARRELL and T. KING, in "Symposium on Effects of Radiation in Structural Materials," ASTM STP 683, edited by J. A. Sprague and D. Kramer (American Society for Testing and Materials, 1979) p. 440.
7. K. FARRELL, *J. Nucl. Materials* **97** (1981) 33.
8. A. MUNITZ, *ibid.* **165** (1989) 305.
9. *Idem*., *ibid.* **165** (1989) 305.
10. H. YOSHIDA, KOZUKA and T. SAGANE, in the 24th Japan Congress on Materials Research-Metallic Materials, Research Reactor Institute Kyoto University, 1981) p. 1.
11. A. MUNITZ, A, STECHMAN, C. COTLER and M. TALIANKER, *J. of Nuclear Materials* **252** (1998) 79.
12. L. F. MONDOLFO, "Aluminum Alloys: Structure and Properties" (Butter Worths, London, 1976.) p. 566.
13. D. A. PORTER and K. E. EASTERLING, "Phase Transformation in Metals and Alloys" (Van Nostrand Rreinhold, UK, 1984) p. 291.
14. D. J. ALEXANDER, in 16 Annual Sym. American Society of Testing and Materials (ASTM), 21–25 June 1992, CONF. 920673-19.
15. E. F. STURCKEN, *J. Nucl. Materials* **82** (1979) 39.

Received 27 January
and accepted 1 September 1999